ELSEVIER

Contents lists available at ScienceDirect

# **Mathematical Biosciences**

journal homepage: www.elsevier.com/locate/mbs



# Original Research Article

# Emergence of non-trivial solutions from trivial solutions in reaction—diffusion equations for pattern formation

Xinyue Evelyn Zhao a,\*, Wenrui Hao b

- a Department of Mathematics, University of Tennessee, Knoxville, TN 37916, USA
- b Department of Mathematics, Pennsylvania State University, University Park, PA, 16802, USA

## ARTICLE INFO

Keywords:
Pattern formation
Reaction–diffusion equations
Bifurcation



Reaction-diffusion equations serve as fundamental tools in describing pattern formation in biology. In these models, nonuniform steady states often represent stationary spatial patterns. Notably, these steady states are not unique, and unveiling them mathematically presents challenges. In this paper, we introduce a framework based on bifurcation theory to address pattern formation problems, specifically examining whether nonuniform steady states can bifurcate from trivial ones. Furthermore, we employ linear stability analysis to investigate the stability of the trivial steady-state solutions. We apply the method to two classic reaction-diffusion models: the Schnakenberg model and the Gray–Scott model. For both models, our approach effectively reveals many nonuniform steady states and assesses the stability of the trivial solution. Numerical computations are also presented to validate the solution structures for these models.

## 1. Introduction

A central challenge in developmental biology is unraveling the mechanisms behind the emergence of spatial and temporal patterns in living organisms [1–4]. Mathematical modeling plays a pivotal role in addressing this complex issue, with both individual-based and continuum models being applied across various contexts [5–7]. One widely employed tool in this field is the use of reaction–diffusion equations to describe molecular interactions and chemical species in biological systems. These equations are especially valuable for elucidating stationary spatial patterns within such systems [8,9].

In reaction–diffusion models featuring multiple species and strongly nonlinear interactions, the theoretical analysis of steady states becomes exceedingly challenging. Computational methods often become indispensable for unraveling the structure and stability of these intricate states. One common approach involves solving the evolutionary system over an extended duration until the solution stabilizes [10]. Nevertheless, it is crucial to acknowledge that this approach does not eliminate the possibility that the obtained solutions are merely metastable. Alternatively, one can directly solve the steady-state system and employ techniques like Newton's method or multigrid methods to tackle the resulting nonlinear system [11–13]. Recently, a deflation technique initially designed for solving polynomial equations has been adapted to

compute multiple solutions and bifurcations of nonlinear partial differential equations [14]. Moreover, a homotopy continuation framework, provides accurate approximations for many, if not all, solutions of the elliptic system without relying on initial guesses [15–17].

Nonetheless, numerical methods can become computationally expensive when dealing with scenarios involving multiple solutions, and they may face challenges in extending to the computation of solutions in three-dimensional domains and large-scale systems. In this paper, we aim to address a fundamental question: Can non-trivial steady states bifurcate from trivial steady states? If this is the case, these seemingly trivial steady-state solutions can provide valuable insights into the global solution structure, as elucidated by analyzing the bifurcation diagram. In systems with homogeneous boundary conditions, one or multiple spatially trivial steady states often exist. Researchers have expended considerable effort in determining whether such systems converge to spatially nonuniform steady states when perturbed from a uniform steady state. A well-known example of this is Turing instability or diffusion-driven instability, which arises from the interaction between a rapidly diffusing activator and a slowly diffusing inhibitor, as explained in [18]. Analyzing this problem typically involves linear stability analysis around the uniform steady state and identifying conditions under which unstable modes emerge, as detailed in [19].

E-mail addresses: xzhao45@utk.edu (X.E. Zhao), wxh64@psu.edu (W. Hao).

https://doi.org/10.1016/j.mbs.2024.109222

Corresponding author.

In this paper, we employ bifurcation theory to address pattern formation problems, specifically, by examining whether non-trivial steady states can bifurcate from seemingly trivial steady states. We also use linear stability analysis to investigate the stability of trivial steady states. Based on the bifurcation and stability analysis, we propose a framework to analyze two-species reaction–diffusion systems. This framework can also be extended to analyze reaction–diffusion models involving n species. To illustrate our approach, we examine two classic models in mathematical biology: the Schnakenberg model, introduced in the 1970s to explain biological pattern formation arising from diffusion-driven instability [20], and the Gray-Scott model, proposed in the 1980s to describe autocatalytic glycolysis reactions [6].

The structure of this paper is as follows: In Section 2, we apply bifurcation theory and linear stability theory to a general reaction—diffusion system featuring two species and explore the solution structures around trivial steady states. The numerical simulation techniques used in this project are also detailed in Section 2. In Sections 3 and 4, we apply the method to the Schnakenberg model and the Gray-Scott model, respectively. We provide a discussion of our result in Section 5.

## 2. Bifurcation and stability analysis

We consider a general reaction–diffusion system for the dynamics of two chemical species, denoted as u and v. In the case of a 1D domain  $x \in [0,1]$  with no-flux boundary conditions, namely:

$$\begin{split} \frac{\partial u}{\partial t} &= D_u \frac{\partial^2 u}{\partial x^2} + f(u, v), \\ \frac{\partial v}{\partial t} &= D_v \frac{\partial^2 v}{\partial x^2} + g(u, v), \end{split} \tag{1}$$

where  $D_u$  and  $D_v$  are the diffusion coefficients, and f(u,v) and g(u,v) are smooth functions representing the reaction terms. Without loss of generality, we let  $D_u=1$  and  $D_v=d$ , and the parameter d measures the relative dispersal speed of the two species.

In the steady-state, the time derivatives are zero, and the equations reduce to:

$$0 = \frac{d^2 u}{dx^2} + f(u, v),$$

$$0 = d\frac{d^2 v}{dx^2} + g(u, v).$$
(2)

Solving the aforementioned system using no-flux boundary conditions leads to steady-state solutions. However, finding explicit solutions for the ODE system (2) in general can be challenging and often necessitates the use of numerical methods. To obtain a simple steady-state solution, we can assume that the concentrations u and v are spatially constant. This assumption implies finding two constants  $u^*$  and  $v^*$  that satisfy the following system of nonlinear equations.

$$f(u^*, v^*) = 0,$$
  
 $g(u^*, v^*) = 0.$  (3)

In this work, we will use bifurcation analysis to find other non-trivial steady-state solutions and reveal the solution structure around the particular steady-state solution  $(u^*, v^*)$ . To achieve this goal, we shall use the Crandall–Rabinowitz theorem. Upon checking the four conditions in the theorem, we can find values for the bifurcation parameter, at which non-constant steady-state solutions bifurcate from the trivial solution.

**Theorem 1** (Crandall–Rabinowitz Theorem, [21,22]). Let X, Y be real Banach spaces and  $\mathcal{F}(\cdot,\cdot)$  be a  $C^p$ ,  $p \geq 2$  map of a neighborhood  $(\mu_0,0)$  in  $\mathbb{R} \times X$  into Y. Denote by  $D_x\mathcal{F}$  and  $D_{\mu x}\mathcal{F}$  the first- and second-order Fréchet derivatives, respectively. Assume the following four conditions hold:

- (I)  $\mathcal{F}(\mu, 0) = 0$  for all  $\mu$  in a neighborhood of  $\mu_0$ ,
- (II) Ker  $D_x \mathcal{F}(\mu_0, 0)$  is one dimensional space, spanned by  $x_0$ ,
- (III) Im  $D_x \mathcal{F}(\mu_0, 0) = Y_1$  has codimension 1,

(IV) 
$$D_{\mu x} \mathcal{F}(\mu_0, 0) x_0 \notin Y_1$$
,

then  $(\mu, x) = (\mu_0, 0)$  is a bifurcation point of the equation  $\mathcal{F}(\mu, x) = 0$  in the following sense: in a neighborhood of  $(\mu, x) = (\mu_0, 0)$ , the set of solutions  $\mathcal{F}(\mu, x) = 0$  consists of two  $C^{p-2}$  smooth curves,  $\Gamma_1$  and  $\Gamma_2$ , which intersect only at the point  $(\mu_0, x) = (\mu_0, 0)$ ;  $\Gamma_1$  is the curve  $x \equiv 0$ , and  $\Gamma_2$  can be parameterized as follows:

$$\Gamma_2$$
:  $(\mu(\epsilon), x(\epsilon)), |\epsilon|$  small,  $(\mu(0), x(0)) = (0, \mu_0), x'(0) = x_0$ .

**Remark 2.1.** We can shift any constant solution to 0, therefore, the Crandall–Rabinowitz Theorem is also valid for any constant solution (see [23]).

#### 2.1. Bifurcation analysis

Different from [23,24], we are now dealing with a system instead of a single function. Therefore, we define

$$\mathcal{F}\left(d, \begin{bmatrix} u \\ v \end{bmatrix}\right) = \begin{bmatrix} u_{xx} + f(u, v) \\ dv_{xx} + g(u, v) \end{bmatrix},\tag{4}$$

where the parameter d is viewed as the bifurcation parameter. Several studies have explored the use of the diffusion coefficient as a bifurcation parameter [25–28]. Additionally, some works have focused on using other parameters for bifurcation analysis [29,30].

Since u and v both satisfy no-flux boundary conditions, we consider the following Banach space

$$X^{l} = \{ \phi(x) \in C^{l}[0, 1], \phi_{x}(0) = \phi_{x}(1) = 0 \}.$$
 (5)

It can be easily proved that the set  $\{\cos(n\pi x)\}_{n=0}^{\infty}$  is a basis for the Banach space  $X^l$  for any  $l \ge 0$ . In applying the Crandall–Rabinowitz Theorem (Theorem 1), we take

$$X = \begin{bmatrix} X^{l+2} \\ X^{l+2} \end{bmatrix} \quad \text{and} \quad Y = \begin{bmatrix} X^l \\ X^l \end{bmatrix}. \tag{6}$$

For any  $x = \begin{bmatrix} u \\ v \end{bmatrix} \in X$ , we consider the infinity vector norm, i.e.,

$$\|\mathbf{x}\|_{X} = \max\{\|\mathbf{u}\|_{X^{l+2}}, \|\mathbf{v}\|_{X^{l+2}}\}.$$
 (7)

It follows from (4) that  $\mathcal{F}$  involves at most second-order derivatives, hence, the operator  $\mathcal{F}$  maps  $\mathbb{R} \times X$  into Y. In addition, recalling that  $(u,v)=(u^*,v^*)$  is a constant steady-state solution, we have

$$\mathcal{F}\left(d,\begin{bmatrix}u^*\\v^*\end{bmatrix}\right) = \begin{bmatrix}0\\0\end{bmatrix} \text{ for any } d > 0.$$

Therefore, the first condition of the Crandall–Rabinowitz Theorem (Theorem 1) is satisfied. Moving forward, we will work on the operator  $\mathcal F$  and find bifurcation points d at which the other three conditions of the Crandall–Rabinowitz Theorem (Theorem 1) are met. To this end, we need the Fréchet derivative of  $\mathcal F$ , which is computed in the following largest

**Lemma 2.1.** The Fréchet derivative  $\mathcal{F}_x\left(d,\begin{bmatrix}u^*\\v^*\end{bmatrix}\right)$  of the operator  $\mathcal{F}$  is given by

$$\mathcal{F}_{\mathbf{x}}\left(d, \begin{bmatrix} u^* \\ v^* \end{bmatrix}\right) \begin{bmatrix} h \\ w \end{bmatrix} = \begin{bmatrix} h_{xx} + f_u(u^*, v^*)h + f_v(u^*, v^*)w \\ dw_{xx} + g_u(u^*, v^*)h + g_v(u^*, v^*)w \end{bmatrix}$$

$$= \begin{bmatrix} 1 & 0 \\ 0 & d \end{bmatrix} \begin{bmatrix} h \\ w \end{bmatrix}_{xx} + \begin{bmatrix} f_u(u^*, v^*) & f_v(u^*, v^*) \\ g_u(u^*, v^*) & g_v(u^*, v^*) \end{bmatrix} \begin{bmatrix} h \\ w \end{bmatrix}. \tag{8}$$

**Proof.** Let  $h, w \in X^{l+2}$  and  $|\varepsilon| \ll 1$ . Using Taylor Series, we have

$$\mathcal{F}\left(d, \begin{bmatrix} u^* \\ v^* \end{bmatrix} + \varepsilon \begin{bmatrix} h \\ w \end{bmatrix}\right) = \mathcal{F}\left(d, \begin{bmatrix} u^* + \varepsilon h \\ v^* + \varepsilon w \end{bmatrix}\right)$$

$$= \begin{bmatrix} (u^* + \varepsilon h)_{xx} + f(u^* + \varepsilon h, v^* + \varepsilon w) \\ d(v^* + \varepsilon w)_{xx} + g(u^* + \varepsilon h, v^* + \varepsilon w) \end{bmatrix}$$

$$= \varepsilon \begin{bmatrix} h_{xx} + f_u(u^*, v^*)h + f_v(u^*, v^*)w \\ dw_{xx} + g_u(u^*, v^*)h + g_v(u^*, v^*)w \end{bmatrix} + \begin{bmatrix} A_1 \\ A_2 \end{bmatrix},$$

$$(9)$$

where

$$\begin{split} A_1 &= \epsilon^2 \bigg( \frac{1}{2} f_{uu}(\eta_1, \xi_1) h^2 + f_{uv}(\eta_1, \xi_1) h w + \frac{1}{2} f_{vv}(\eta_1, \xi_1) w^2 \bigg) \\ &= \frac{\epsilon^2}{2} \left[ h \quad w \right] \begin{bmatrix} f_{uu}(\eta_1, \xi_1) & f_{uv}(\eta_1, \xi_1) \\ f_{uv}(\eta_1, \xi_1) & f_{vv}(\eta_1, \xi_1) \end{bmatrix} \begin{bmatrix} h \\ w \end{bmatrix} \end{split}$$

and

$$\begin{split} A_2 &= \varepsilon^2 \bigg( \frac{1}{2} g_{uu}(\eta_2, \xi_2) h^2 + g f_{uv}(\eta_2, \xi_2) h w + \frac{1}{2} g_{vv}(\eta_2, \xi_2) w^2 \bigg) \\ &= \frac{\varepsilon^2}{2} \begin{bmatrix} h & w \end{bmatrix} \begin{bmatrix} g_{uu}(\eta_2, \xi_2) & g_{uv}(\eta_2, \xi_2) \\ g_{uv}(\eta_2, \xi_2) & g_{vv}(\eta_2, \xi_2) \end{bmatrix} \begin{bmatrix} h \\ w \end{bmatrix} \end{split}$$

are the remainder terms. In the above two equations,  $\eta_1, \eta_2$  are between  $u^*$  and  $u^* + \varepsilon h$ , and  $\xi_1, \xi_2$  lie between  $v^*$  and  $v^* + \varepsilon w$ .

Since functions f and g are both second-order differentiable, all the second-order derivative terms in  $A_1$  and  $A_2$  are bounded. Therefore,

$$\begin{aligned} \|A_1\|_Y &= \|A_1\|_{X^l} \le C\varepsilon^2 (\max\{\|h\|_{X^l}, \|w\|_{X^l}\})^2 \\ &\le C\varepsilon^2 (\max\{\|h\|_{X^{l+2}}, \|w\|_{X^{l+2}}\})^2 = C\varepsilon^2 \left\| \begin{bmatrix} h \\ w \end{bmatrix} \right\|_{Y}^2, \end{aligned}$$

and so does  $A_2$ .

Combining the estimates on  $A_1$  and  $A_2$  with (9), we arrive

$$\frac{\left\|\mathcal{F}\left(d,\begin{bmatrix}u^*\\v^*\end{bmatrix}+\varepsilon\begin{bmatrix}h\\w\end{bmatrix}\right)-\mathcal{F}\left(d,\begin{bmatrix}u^*\\v^*\end{bmatrix}\right)-\varepsilon\begin{bmatrix}\left(u^*+\varepsilon h\right)_{xx}+f(u^*+\varepsilon h,v^*+\varepsilon w)\\d(v^*+\varepsilon w)_{xx}+g(u^*+\varepsilon h,v^*+\varepsilon w)\end{bmatrix}\right\|_Y}{\varepsilon\left\|\begin{bmatrix}h\\w\end{bmatrix}\right\|_X}$$

$$= \frac{\left\| \begin{bmatrix} A_1 \\ A_2 \end{bmatrix} \right\|_Y}{\varepsilon \left\| \begin{bmatrix} h \\ w \end{bmatrix} \right\|_X} = \frac{\max\{\|A_1\|_{X^I}, \|A_2\|_{X^I}\}}{\varepsilon \left\| \begin{bmatrix} h \\ w \end{bmatrix} \right\|_X} \le C\varepsilon \left\| \begin{bmatrix} h \\ w \end{bmatrix} \right\|_X \to 0 \quad \text{as } \varepsilon \to 0,$$

which concludes (8).

Since the set  $\{\cos(n\pi x)\}_{n=0}^{\infty}$  is a basis for the Banach space  $X^{l+2}$ , for any  $h,w\in X^{l+2}$ , we write

$$\begin{bmatrix} h \\ w \end{bmatrix} = \begin{bmatrix} \sum_{n=0}^{\infty} a_{n1} \cos(n\pi x) \\ \sum_{n=0}^{\infty} a_{n2} \cos(n\pi x) \end{bmatrix} = \sum_{n=0}^{\infty} \cos(n\pi x) \left( a_{n1} \begin{bmatrix} 1 \\ 0 \end{bmatrix} + a_{n2} \begin{bmatrix} 0 \\ 1 \end{bmatrix} \right)$$
$$= \sum_{n=0}^{\infty} a_{n2} \cos(n\pi x) \begin{bmatrix} b_n \\ 1 \end{bmatrix}$$
(10)

where  $b_n = \frac{a_{n1}}{a_{n2}}$ , and  $a_{n1}, a_{n2}$  are arbitrary constants. We can see that, for each  $\cos(n\pi x)$ , there exists a 2-dimensional space.

To analyze the kernel of  $\mathcal{F}_x$ , we substitute (10) into (8) to derive

$$\begin{split} &\mathcal{F}_x\left(d,\begin{bmatrix}u^*\\v^*\end{bmatrix}\right)\begin{bmatrix}h\\w\end{bmatrix} = \mathcal{F}_x\left(d,\begin{bmatrix}u^*\\v^*\end{bmatrix}\right)\left(\sum_{n=0}^\infty a_{n2}\cos(n\pi x)\begin{bmatrix}b_n\\1\end{bmatrix}\right) \\ &= \sum_{n=0}^\infty a_{n2}\left(-n^2\pi^2\begin{bmatrix}1&0\\0&d\end{bmatrix} + \begin{bmatrix}f_u(u^*,v^*)&f_v(u^*,v^*)\\g_u(u^*,v^*)&g_v(u^*,v^*)\end{bmatrix}\right)\cos(n\pi x)\begin{bmatrix}b_n\\1\end{bmatrix} \\ &= \sum_{n=0}^\infty a_{n2}\cos(n\pi x)\begin{bmatrix}-n^2\pi^2 + f_u(u^*,v^*)&f_v(u^*,v^*)\\g_u(u^*,v^*)&-n^2\pi^2d + g_v(u^*,v^*)\end{bmatrix}\begin{bmatrix}b_n\\1\end{bmatrix}. \end{split}$$

In particular,

$$\begin{split} &\mathcal{F}_x \left( d, \begin{bmatrix} u^* \\ v^* \end{bmatrix} \right) \cos(n\pi x) \begin{bmatrix} b_n \\ 1 \end{bmatrix} \\ &= \cos(n\pi x) \begin{bmatrix} -n^2\pi^2 + f_u(u^*, v^*) & f_v(u^*, v^*) \\ g_u(u^*, v^*) & -n^2\pi^2 d + g_v(u^*, v^*) \end{bmatrix} \begin{bmatrix} b_n \\ 1 \end{bmatrix}. \end{split}$$

When  $\left(-n^2\pi^2 + f_u(u^*, v^*)\right)\left(-n^2\pi^2d + g_v(u^*, v^*)\right) - f_v(u^*, v^*)g_u(u^*, v^*) = 0$ , i.e.

$$d = d_n^* \triangleq \frac{\frac{f_v(u^*, v^*)g_u(u^*, v^*)}{n^2\pi^2 - f_u(u^*, v^*)} + g_v(u^*, v^*)}{n^2\pi^2} \qquad n \ge 1,$$
(11)

the matrix  $\begin{bmatrix} -n^2\pi^2 + f_u(u^*,v^*) & f_v(u^*,v^*) \\ g_u(u^*,v^*) & -n^2\pi^2d + g_v(u^*,v^*) \end{bmatrix}$  is singular and has a non-trivial element in its nullspace. In order to identity the nullspace, we derive from

$$\begin{bmatrix} -n^2\pi^2 + f_u(u^*, v^*) & f_v(u^*, v^*) \\ g_u(u^*, v^*) & -n^2\pi^2d_n^* + g_v(u^*, v^*) \end{bmatrix} \begin{bmatrix} b_n \\ 1 \end{bmatrix} = \begin{bmatrix} 0 \\ 0 \end{bmatrix}$$
 (12)

tha

$$b_n = b_n^* \triangleq \frac{f_v(u^*, v^*)}{n^2 \pi^2 - f_u(u^*, v^*)}.$$
 (13)

In this case, we have  $\begin{bmatrix} b_n^* \\ 1 \end{bmatrix} \in \mathcal{N} \left( \begin{bmatrix} -n^2\pi^2 + f_u(u^*, v^*) & f_v(u^*, v^*) \\ g_u(u^*, v^*) & -n^2\pi^2d_n^* + g_v(u^*, v^*) \end{bmatrix} \right)$ , and  $\cos(n\pi x) \begin{bmatrix} b_n^* \\ 1 \end{bmatrix} \in \operatorname{Ker} \mathcal{F}_x \left( d_n^*, \begin{bmatrix} u^* \\ v^* \end{bmatrix} \right)$ . Moreover, it follows from the expression of (13) that  $b_n^*$  is decreasing in n. So,

$$b_n^* \neq b_m^* \text{ when } n \neq m. \tag{14}$$

For  $d_n^*$ , even though the monotonicity in n cannot be proved, it is usually the case that

$$d_n^* \neq d_m^* \text{ when } n \neq m. \tag{15}$$

If (15) holds, then

$$\operatorname{Ker} \mathcal{F}_{x}\left(d_{n}^{*}, \begin{bmatrix} u^{*} \\ v^{*} \end{bmatrix}\right) = \operatorname{Span}\left\{\cos(n\pi x) \begin{bmatrix} b_{n}^{*} \\ 1 \end{bmatrix}\right\}$$

is a 1-dimensional space. Hence, the second requirement of the Crandall–Rabinowitz Theorem (Theorem 1) is satisfied at  $d=d_n^*$  with  $n\geq 1$ . In order to check the codimension of  $\operatorname{Im} \mathcal{F}_x\Bigl(d_n^*, \begin{bmatrix} u^* \\ v^* \end{bmatrix}\Bigr)$  in the third condition of Theorem 1, we recall

$$\begin{split} &\mathcal{F}_{\mathbf{x}}\left(d_{n}^{*}, \begin{bmatrix} u^{*} \\ v^{*} \end{bmatrix}\right) \begin{bmatrix} h \\ w \end{bmatrix} \\ &= \sum_{m=0}^{\infty} a_{m2} \cos(m\pi x) \begin{bmatrix} -m^{2}\pi^{2} + f_{u}(u^{*}, v^{*}) & f_{v}(u^{*}, v^{*}) \\ g_{u}(u^{*}, v^{*}) & -m^{2}\pi^{2}d_{n}^{*} + g_{v}(u^{*}, v^{*}) \end{bmatrix} \begin{bmatrix} b_{m} \\ 1 \end{bmatrix}. \end{split}$$

If (15) holds, then

$$\det \left( \begin{bmatrix} -m^2\pi^2 + f_u(u^*, v^*) & f_v(u^*, v^*) \\ g_u(u^*, v^*) & -m^2\pi^2d_n^* + g_v(u^*, v^*) \end{bmatrix} \right) \neq 0,$$

when  $m \neq n$ . This indicates that for  $m = 0, 1, 2, \cdots$  and  $m \neq n$ , the matrix is nonsingular, and the 2-dimensional space corresponding to  $\cos(m\pi x)$  remains. On the other hand, when m = n, following our previous analysis, the subspace spanned by  $\begin{bmatrix} b_n^* \\ 1 \end{bmatrix} \cos(n\pi x)$  is in the kernel

of 
$$\mathcal{F}_x\left(d_n^*, \begin{bmatrix} u^* \\ v^* \end{bmatrix}\right)$$
, hence it is not in the image space of  $\mathcal{F}_x\left(d_n^*, \begin{bmatrix} u^* \\ v^* \end{bmatrix}\right)$ .

Therefore, only one dimension disappears and  $\operatorname{Im} \mathcal{F}_{\mathbf{x}}\left(d_{n}^{*}, \begin{bmatrix} u^{*} \\ v^{*} \end{bmatrix}\right)$  has codimension 1.

Finally, taking  $d = d_n^*$ , we differentiate both sides of (8) with respect to d and apply the operator on  $\cos(n\pi x) \begin{bmatrix} b_n^* \\ 1 \end{bmatrix}$ . We obtain, with  $n \ge 1$ ,

$$\mathcal{F}_{dx}\left(d_n^*, \begin{bmatrix} u^* \\ v^* \end{bmatrix}\right) \cos(n\pi x) \begin{bmatrix} b_n^* \\ 1 \end{bmatrix} = \begin{bmatrix} 0 \\ -n^2\pi^2 \cos(n\pi x) \end{bmatrix} = \cos(n\pi x) \begin{bmatrix} 0 \\ -n^2\pi^2 \end{bmatrix}.$$

We shall prove the last condition of the Crandall–Rabinowitz Theorem (Theorem 1) by contradiction. We assume that

$$\mathcal{F}_{dx}\left(d_n^*, \begin{bmatrix} u^* \\ v^* \end{bmatrix}\right) \cos(n\pi x) \begin{bmatrix} b_n^* \\ 1 \end{bmatrix} \in \operatorname{Im} \, \mathcal{F}_x\left(d_n^*, \begin{bmatrix} u^* \\ v^* \end{bmatrix}\right). \tag{16}$$

That means there is a nonzero vector  $z = \begin{bmatrix} z_1 \\ z_2 \end{bmatrix} \in X$  such that

$$\mathcal{F}_{x}\left(d_{n}^{*},\begin{bmatrix}u^{*}\\v^{*}\end{bmatrix}\right)\begin{bmatrix}z_{1}\\z_{2}\end{bmatrix}=\mathcal{F}_{dx}\left(d_{n}^{*},\begin{bmatrix}u^{*}\\v^{*}\end{bmatrix}\right)\cos(n\pi x)\begin{bmatrix}b_{n}^{*}\\1\end{bmatrix}=\cos(n\pi x)\begin{bmatrix}0\\-n^{2}\pi^{2}\end{bmatrix}.$$

Using (8), we find that it is equivalent to

$$\begin{bmatrix} 1 & 0 \\ 0 & d_n^* \end{bmatrix} \begin{bmatrix} z_1 \\ z_2 \end{bmatrix}_{xx} + \begin{bmatrix} f_u(u^*, v^*) & f_v(u^*, v^*) \\ g_u(u^*, v^*) & g_v(u^*, v^*) \end{bmatrix} \begin{bmatrix} z_1 \\ z_2 \end{bmatrix} = \cos(n\pi x) \begin{bmatrix} 0 \\ -n^2 \pi^2 \end{bmatrix}.$$
(17)

Since the right-hand side contains only  $\cos(n\pi x)$ , we use the ansatz:

$$z_1 = a_1 \cos(n\pi x)$$
 and  $z_2 = a_2 \cos(n\pi x)$ 

Upon substituting into (17), we obtain

$$\begin{bmatrix} 1 & 0 \\ 0 & d_n^* \end{bmatrix} \begin{bmatrix} -n^2 \pi^2 a_1 \cos(n\pi x) \\ -n^2 \pi^2 a_2 \cos(n\pi x) \end{bmatrix} + \begin{bmatrix} f_u(u^*, v^*) & f_v(u^*, v^*) \\ g_u(u^*, v^*) & g_v(u^*, v^*) \end{bmatrix} \begin{bmatrix} a_1 \cos(n\pi x) \\ a_2 \cos(n\pi x) \end{bmatrix}$$

$$= \cos(n\pi x) \begin{bmatrix} 0 \\ -n^2 \pi^2 \end{bmatrix}, \tag{18}$$

which is equivalent to solving the linear system

$$\begin{bmatrix} -n^2\pi^2 + f_u(u^*, v^*) & f_v(u^*, v^*) \\ g_u(u^*, v^*) & -n^2\pi^2 d_n^* + g_v(u^*, v^*) \end{bmatrix} \begin{bmatrix} a_1 \\ a_2 \end{bmatrix} = \begin{bmatrix} 0 \\ -n^2\pi^2 \end{bmatrix}.$$
 (19)

We first consider the case when  $a_2=0.$  Then the first equation of the system (19) is reduced to

$$\left(-n^2\pi^2 + f_u(u^*, v^*)\right)a_1 = 0, (20)$$

which gives  $a_1=0$ . Here, we exclude the scenario where  $-n^2\pi^2+f_u(u^*,v^*)=0$ ; in our bifurcation diagrams (Figs. 1, 4, and 5), this condition manifests as asymptotes. Then the second equation of (19) cannot be satisfied, and we have found a contradiction.

When  $a_2 \neq 0$ , we divide both sides of (19) by  $a_2$ . Alternatively, we can solve (19) by

$$\begin{bmatrix} -n^2\pi^2 + f_u(u^*, v^*) & f_v(u^*, v^*) \\ g_u(u^*, v^*) & -n^2\pi^2d_n^* + g_v(u^*, v^*) \end{bmatrix} \begin{bmatrix} \frac{a_1}{a_2} \\ 1 \end{bmatrix} = \begin{bmatrix} 0 \\ \frac{-n^2\pi^2}{a_2} \end{bmatrix}.$$
(21)

Comparing (21) with (12), we find that the first equations from the two systems are the same, so they should admit the same solution, i.e.,  $\frac{a_1}{a_2} = b_n^*$ . However, from the second equation in (12), we have

$$g_u(u^*, v^*) \frac{a_1}{a_2} + \left(-n^2 \pi^2 d_n^* + g_v(u^*, v^*)\right) = 0 \neq \frac{-n^2 \pi^2}{a_2},$$

when  $n \ge 1$ . So, we have found a contradiction, and the assumption (16) is not valid.

In conclusion, based on the above analysis, the four conditions of the Crandall–Rabinowitz Theorem (Theorem 1) are satisfied at  $d=d_n^*$  when the condition (15) is met. Therefore,  $d=d_n^*$  is a bifurcation point of the system (2), at which a non-constant solution bifurcates from the trivial steady state  $(u,v)=(u^*,v^*)$ . We summarize our result into the following theorem:

**Theorem 2.1.** If (15) holds, then for each integer  $n \ge 1$ ,  $d = d_n^*$ , where  $d_n^*$  is defined in (11), is a bifurcation point to the system (2). In addition, the bifurcation solution  $(u_n(x, \varepsilon), v_n(x, \varepsilon), d_n(\varepsilon))$  satisfies

$$d_n(\varepsilon) = d_n^* + \varepsilon, \qquad u_n(x, \varepsilon) = u^* + \varepsilon b_n^* \cos(n\pi x) + o(\varepsilon),$$
  
$$v_n(x, \varepsilon) = v^* + \varepsilon \cos(n\pi x) + o(\varepsilon),$$

where  $b_{\epsilon}^*$  is defined in (13) and  $|\epsilon| \ll 1$ .

## 2.2. Linear stability analysis

To gain a deeper insight into the solution structure, we may conduct a linear stability analysis focused on constant steady-state solutions. While both stability and bifurcation are important concepts in a system, they are not isolated from each other. Stability refers to the ability of the system to maintain its preferred state, while bifurcation refers to the tendency of the system to transition into a different state with the change of a parameter. It is often at the bifurcation points that the stability of the constant solution changes. As highlighted by Crandall

and Rabinowitz in their seminal work [31], assessing the stability of a constant solution necessitates the estimation of the eigenvalue with the minimum modulus from the linearized operator associated with the bifurcation. In our previous research [24,32–34], we also found that in many cases (though not all), the change of stability for the system coincides with the smallest bifurcation point. Studying these two interconnected concepts will provide us with an in-depth understanding of the system and its solution structure.

Here we carry out the standard linear stability analysis. Assume that the initial conditions are perturbed as follows:

$$u_0(x) = u^* + \varepsilon h_0(x), \qquad v_0(x) = v^* + \varepsilon w_0(x).$$

Substituting

$$u(x,t) = u^* + \varepsilon h(x,t) + O(\varepsilon^2), \qquad v(x,t) = v^* + \varepsilon w(x,t) + O(\varepsilon^2)$$

into (1) and collecting the  $\epsilon$ -order terms, we obtain the linearized system of (1) at the constant steady-state solution:

$$h_t = h_{xx} + f_u(u^*, v^*)h + f_v(u^*, v^*)w,$$
  

$$w_t = dw_{xx} + g_u(u^*, v^*)h + g_v(u^*, v^*)w.$$
(22)

Since both h and w also satisfy no-flux boundary conditions, we seek a solution of the form

$$h(x,t) = \sum_{n=0}^{\infty} h_n(t) \cos(n\pi x), \qquad w(x,t) = \sum_{n=0}^{\infty} w_n(t) \cos(n\pi x).$$

Substituting back into (22), we obtain

$$h'_n(t) = -n^2 \pi^2 h_n(t) + f_u(u^*, v^*) h_n(t) + f_v(u^*, v^*) w_n(t),$$

$$w'_n(t) = -dn^2 \pi^2 w_n(t) + g_n(u^*, v^*) h_n(t) + g_n(u^*, v^*) w_n(t),$$
(23)

which is equivalent to the matrix equation

$$\begin{bmatrix} h_n(t) \\ w_n(t) \end{bmatrix}' = \begin{bmatrix} -n^2 \pi^2 + f_u(u^*, v^*) & f_v(u^*, v^*) \\ g_u(u^*, v^*) & -dn^2 \pi^2 + g_v(u^*, v^*) \end{bmatrix} \begin{bmatrix} h_n(t) \\ w_n(t) \end{bmatrix}.$$
 (24)

We denote  $\mathbf{x} = \begin{bmatrix} h_n(t) \\ w_n(t) \end{bmatrix}$  and  $\mathbf{A} = \begin{bmatrix} -n^2\pi^2 + f_u(u^*, v^*) & f_v(u^*, v^*) \\ g_u(u^*, v^*) & -dn^2\pi^2 + g_v(u^*, v^*) \end{bmatrix}$ . The solution to the matrix differential equation (24) is

$$\mathbf{x} = c_1 e^{\lambda_1 t} \mathbf{x_1} + c_2 e^{\lambda_2 t} \mathbf{x_2},$$

where  $\lambda_1$ ,  $\lambda_2$  are the eigenvalues of the matrix A,  $x_1$ ,  $x_2$  are the respective eigenvectors, and  $c_1$ ,  $c_2$  are constants which are determined by the initial conditions  $h_0(x)$ ,  $w_0(x)$ . It is clear that  $x \to 0$  if and only if the two eigenvalues are negative. Therefore, the stability of the constant steady-state solution depends on the signs of the eigenvalues of A.

**Theorem 2.2.** The constant steady-state solution  $(u^*, v^*)$  is linearly stable if and only if

$$\lambda_1 + \lambda_2 = tr(A) = -n^2 \pi^2 + f_{\nu}(u^*, v^*) - dn^2 \pi^2 + g_{\nu}(u^*, v^*) < 0, \tag{25}$$

$$\lambda_1 \lambda_2 = \det(A) = \left(-n^2 \pi^2 + f_u(u^*, v^*)\right) \left(-dn^2 \pi^2 + g_v(u^*, v^*)\right) - f_v(u^*, v^*) g_u(u^*, v^*) > 0,$$
(26)

hold for all integers  $n \ge 0$ .

#### 2.3. Numerical homotopy continuation techniques

To numerically approximate the operator  $\mathcal{F}$  defined in (4), denoted as  $\mathcal{F}^h$  where h is the mesh size of numerical discretization, we solve the following discretized nonlinear system:

$$\mathcal{F}^h\left(d, \begin{bmatrix} u^h \\ v^h \end{bmatrix}\right) = \mathbf{0}.$$

Here,  $\mathcal{F}^h: \mathbb{R} \times \mathbb{R}^{2n} \to \mathbb{R}^{2n}$  and  $\begin{bmatrix} u^h \\ v^h \end{bmatrix}$  is the numerical approximation of  $\begin{bmatrix} u \\ v \end{bmatrix}$  in (4) depending on the parameter d, i.e.,  $\begin{bmatrix} u^h \\ v^h \end{bmatrix} = \begin{bmatrix} u^h(d) \\ v^h(d) \end{bmatrix}$ . Starting

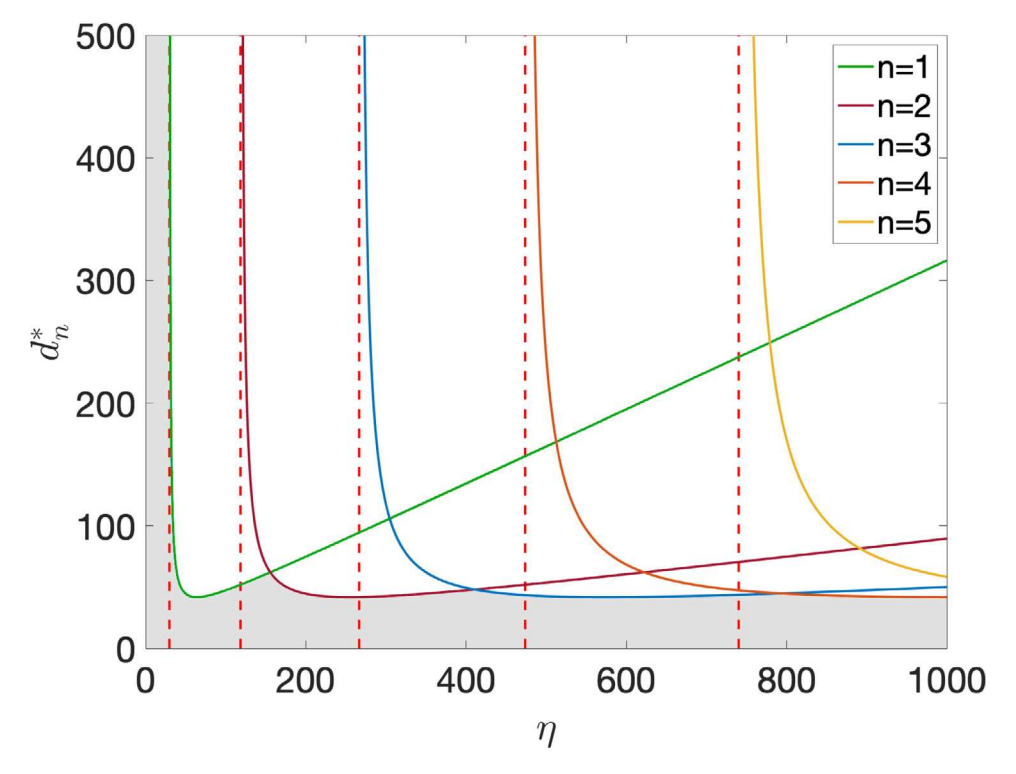


Fig. 1. The relationship between  $d_u^*$  and  $\eta$  from Equation (28). Dashed curves indicate asymptotes. Curves with different colors represent different bifurcation branches. The number of bifurcation points is equal to the number of intersections with a vertical line. The constant solution  $(u^*, v^*) = (1, \frac{2}{3})$  is linearly stable within the shaded region. Other parameter values used are:  $a = \frac{1}{3}$  and  $b = \frac{2}{3}$ .

with the linearized solution around a bifurcation point provided by Theorem 2.1, i.e.,  $\begin{bmatrix} u_0 \\ v_0 \end{bmatrix} = \begin{bmatrix} u^h(d_0) \\ v^h(d_0) \end{bmatrix}, \text{ we can employ various homotopy tracking algorithms, as discussed in previous literature [35–37], to compute the solution path <math display="block">\begin{bmatrix} u^h(d) \\ v^h(d) \end{bmatrix}.$  The homotopy tracking algorithm typically consists of a predictor step followed by a corrector step to solve the parametric problem. The predictor computes the solution at  $d_1 = d_0 + \Delta d$  by solving

$$\mathcal{F}^h\bigg(d_0 + \Delta d, \begin{bmatrix} u_0^h + \Delta u^h \\ v_0^h + \Delta v^h \end{bmatrix}\bigg) = 0$$

which, in first order, yields an Euler predictor:

$$\mathcal{F}^h_x \left( d_0, \begin{bmatrix} u_0 \\ v_0 \end{bmatrix} \right) \begin{bmatrix} \Delta u^h \\ \Delta v^h \end{bmatrix} = -\mathcal{F}^h_d \left( d_0, \begin{bmatrix} u_0 \\ v_0 \end{bmatrix} \right) \Delta d.$$

Subsequently, a Newton corrector is applied to refine the solution using an initial guess  $\begin{bmatrix} \widetilde{u}^h \\ \widetilde{v}^h \end{bmatrix} = \begin{bmatrix} u_0 + \Delta u^h \\ v_0 + \Delta v^h \end{bmatrix}$ , namely,

$$\mathcal{F}_{x}^{h}\left(d_{1},\begin{bmatrix}\widetilde{u}^{h}\\\widetilde{v}^{h}\end{bmatrix}\right)\begin{bmatrix}\Delta u^{h}\\\Delta v^{h}\end{bmatrix} = -\mathcal{F}^{h}\left(d_{1},\begin{bmatrix}\widetilde{u}^{h}\\\widetilde{v}^{h}\end{bmatrix}\right)$$

This process iteratively updates  $\begin{bmatrix} \widetilde{u}^h \\ \widetilde{v}^h \end{bmatrix}$  until it lies on the path, i.e.,  $\mathcal{F}^h \left( d_1, \begin{bmatrix} \widetilde{u}^h \\ \widetilde{v}^h \end{bmatrix} \right) = 0.$ 

# 3. Application to the Schnakenberg Turing model

In this section, we apply our framework to the Schnakenberg model, a system whose bifurcation and stability analysis have previously been explored in [38,39]. The Schnakenberg system is a prototype Turing model that exhibits Turing pattern formation. The model involves two variables, u as an activator and v as a substrate. The following equations

can describe the model:

$$\frac{\partial u}{\partial t} = \frac{\partial^2 u}{\partial x^2} + \eta(a - u + u^2 v), 
\frac{\partial v}{\partial t} = d \frac{\partial^2 v}{\partial x^2} + \eta(b - u^2 v).$$
(27)

In this system, both species are produced uniformly in the domain. The variable u decays linearly, while the conversion of v to u occurs in a nonlinear and autocatalytic manner. The diffusion rate d differentiates the relative dispersal speed of the two species, and the parameter  $\eta$  determines the balance between diffusion and chemical reaction.

Comparing (27) with (1), we have

$$f(u, v) = \eta(a - u + u^2 v),$$
  

$$g(u, v) = \eta(b - u^2 v),$$

and the trivial steady-state solution which satisfies (3) is  $(u^*, v^*) = \left(a+b, \frac{b}{(a+b)^2}\right)$ . Taking partial derivatives and evaluating at  $(u^*, v^*)$ , we obtain

$$\begin{split} &f_u(u^*, v^*) = \eta(-1 + 2u^*v^*), \\ &f_v(u^*, v^*) = \eta(u^*)^2, \\ &g_u(u^*, v^*) = -2\eta u^*v^*, \\ &g_v(u^*, v^*) = -\eta(u^*)^2. \end{split}$$

On the basis of Theorem 2.1, we find a series of values for the bifurcation parameter d,

$$d_n^* = \frac{2\eta u^* v^* \frac{\eta(u^*)^2}{\eta(2u^*v^*-1) - n^2\pi^2} - \eta(u^*)^2}{n^2\pi^2} \qquad n \ge 1.$$
 (28)

In the above formula, both the parameters  $\eta$  and d are positive and the solutions  $u^*$  and  $v^*$  are also positive. We will now proceed to discuss the number of bifurcation points based on different scenarios.

• Case 1. If  $2u^*v^* - 1 \le 0$ , then  $\eta(2u^*v^* - 1) - n^2\pi^2 < 0$  for all  $n \ge 1$ . In this case, the numerator of (28) is negative, and so are all the

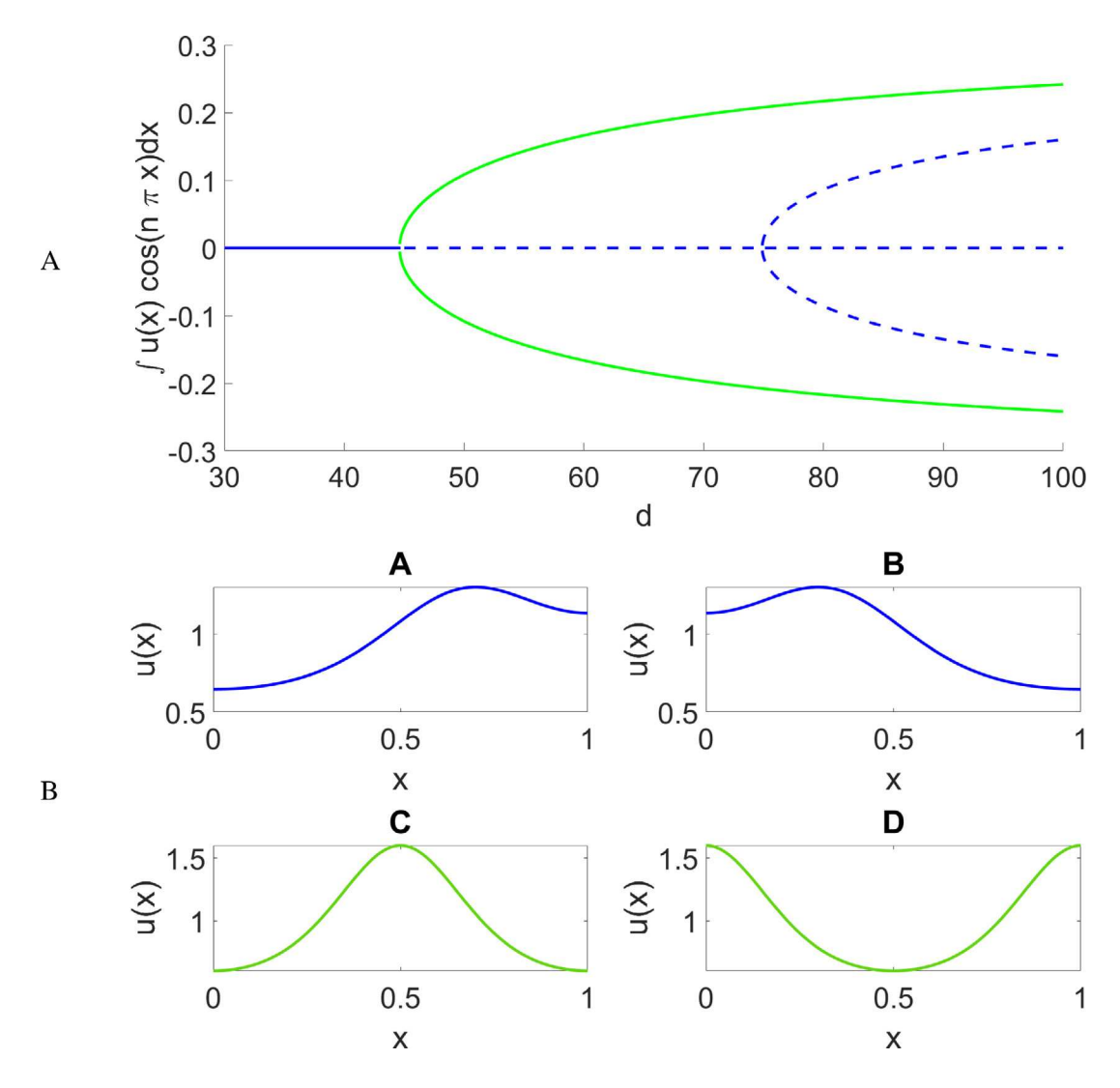


Fig. 2. Steady states of the Schnakenberg model with  $\eta=200$ . A: Bifurcation diagram of the model. The *y*-axis represents  $\int u(x)\cos(n\pi x)\,\mathrm{d}x$ , where u(x) are steady-state solutions. Solid lines indicate stable solutions, while dashed lines indicate unstable solutions. B: Steady-state solutions with d=100 for each solution branch depicted in A. Other parameter values used are:  $a=\frac{1}{3}$  and  $b=\frac{2}{3}$ .

points defined by (28). Therefore, there are no bifurcation points for d>0.

- Case 2. If  $2u^*v^* 1 > 0$ , then  $\eta = \eta_n^* \triangleq \frac{n^2\pi^2}{2u^*v^* 1}$  is an asymptote for  $d_n^*$ , before which  $d_n^*$  is negative and after which  $d_n^*$  is positive. Since we are focusing on d > 0 only, we further discuss the scenarios based on the value of  $\eta$ :
  - If  $0 < \eta < \eta_1^*$ , there is 0 bifurcation point for d;
  - If  $\eta_1^* < \eta \le \eta_2^*$ , there is 1 bifurcation point for d;
  - If  $\eta_2^* < \eta \le \eta_3^*$ , there are 2 bifurcation points for d;
  - ...
  - If  $\eta_{n-1}^* < \eta \le \eta_n^*$ , there are n-1 bifurcation points for d.

When  $a=\frac{1}{3}$  and  $b=\frac{2}{3}$ , then  $u^*=a+b=1$  and  $v^*=\frac{b}{(a+b)^2}=\frac{2}{3}$ . Fig. 1 shows the relationship between the bifurcation point  $d_n^*$  and  $\eta$ , as described in Eq. (28). Curves with different colors represent different bifurcation branches. In addition, the number of bifurcation points at each  $\eta$  value equals the number of intersections with the vertical line  $x=\eta$ .

As for the stability of the constant steady-state solution  $(u^*, v^*) = (1, \frac{2}{3})$ , we use Theorem 2.2 to derive the two conditions required for the constant solution to be stable:

$$-n^{2}\pi^{2} - dn^{2}\pi^{2} + \eta(2u^{*}v^{*} - 1) - \eta(u^{*})^{2} = -n^{2}\pi^{2} - dn^{2}\pi^{2} - \frac{2}{3}\eta < 0,$$
 (29) 
$$\left(\eta(2u^{*}v^{*} - 1) - n^{2}\pi^{2}\right)\left(-\eta(u^{*})^{2} - dn^{2}\pi^{2}\right) + 2\eta^{2}(u^{*})^{3}v^{*}$$

$$= (\frac{\eta}{3} - n^2 \pi^2)(-\eta - dn^2 \pi^2) + \frac{4\eta^2}{3} > 0.$$
 (30)

Clearly, (29) is always satisfied for all  $n \ge 0$ , and (30) holds when n = 0, it then remains to check (30) for different d values and integers  $n \ge 1$ . Recall that  $d = d_n^*$  from (28) makes the left-hand side of (30) equal to 0 for each  $n \ge 1$ . We define

$$d^*(\eta) = \min_{n \ge 1} d_n^*. \tag{31}$$

Here, we would like to emphasize that  $d^*$  depends on  $\eta$ . It can be proved that when  $d < d_*(\eta)$ , (30) always holds for all  $n \ge 1$ , thus  $(u^*, v^*)$  is linearly stable (see the shaded region in Fig. 1); however, when  $d > d_*(\eta)$ , there exists an integer  $n_0$  such that (30) is violated at

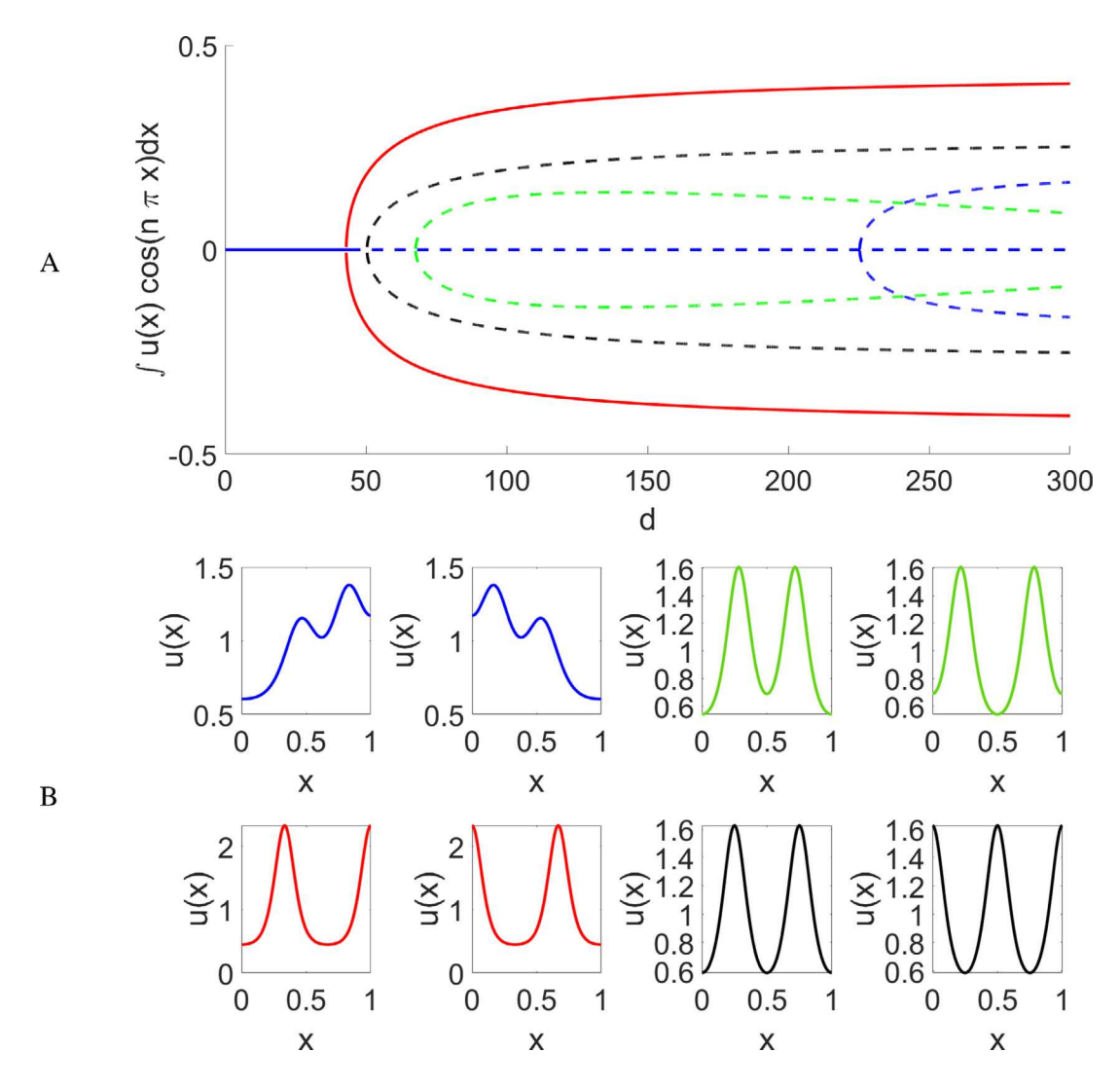


Fig. 3. Steady states of the Schnakenberg model with  $\eta = 700$ . A: Bifurcation diagram of the model. The *y*-axis represents  $\int u(x) \cos(n\pi x) \, dx$ , where u(x) are steady-state solutions. Solid lines indicate stable solutions, while dashed lines indicate unstable solutions. B: Steady-state solutions with d = 300 for each solution branch distinguished by different colors. Other parameter values used are:  $a = \frac{1}{3}$  and  $b = \frac{2}{3}$ .

 $n=n_0$ , thus  $(u^*,v^*)$  is unstable. It indicates that the stability of  $(u^*,v^*)$  changes at the smallest bifurcation point.

We then conduct numerical simulations to explore the steady-state solutions of the Schnakenberg model (27) in a 1D domain  $x \in [0,1]$  with no-flux boundary conditions. Initially, we set the parameter values to  $a=\frac{1}{3},\ b=\frac{2}{3},\$ and  $\eta=200.$  From Fig. 1, we know that there should be 2 bifurcation points, one corresponds to n=1, and the other one corresponds to n=2. Using (28), one can also compute the values of the two bifurcation points:  $d_1^*=74.8779$  and  $d_2^*=44.6227$ . Since  $d_2^*< d_1^*$ , one would expect that the change of stability happens at  $d^*=d_2^*=44.6227$ .

From the simulation results, the bifurcation diagram concerning the diffusion rate d is presented in Fig. 2A. The bifurcation points corresponding to n=1 and n=2 are observed, with respective values of  $d_1^*\approx 75$  and  $d_2^*\approx 45$ . Stable solutions are represented by solid lines, and unstable solutions are depicted with dashed lines. We observe that before the smallest bifurcation point  $d_2^*$  the constant solution is stable, whereas after  $d_2^*$ , the constant solution is unstable. To further analyze the system, we plot the steady-state solutions for d=100 in Fig. 2B. The first two steady-state solutions, plotted in blue, are on the n=1 bifurcation branch, since only one peak and one valley are observed in

the interval [0, 1]. The two green steady-state solutions show either two valleys and one peak or two peaks and one valley, thus they are on the n=2 bifurcation branch. All the simulation results agree well with the analytical results.

Next, we increase the value of the parameter  $\eta$  to  $\eta=700$ , which results in an increase in the number of bifurcations to 4 (namely,  $n=1,\ldots,4$ ). The corresponding bifurcation diagram is shown in Fig. 3A. Additionally, Fig. 3B displays the steady-state solutions for d=300 on each solution branch. We see that the constant steady-state solution changes stability at the smallest bifurcation point  $d^*=d_3^*\approx 43$ .

# 4. Application to the Gray-Scott model

The Gray-Scott model, first proposed by Gray and Scott [40–42], is a reaction–diffusion system used to describe autocatalytic reactions. It models the interaction of two chemicals that react with each other and diffuse through space, leading to complex patterns such as spirals, spots, and waves. In 1D, it takes the following form:

$$\begin{split} \frac{\partial A}{\partial t} &= D_A \frac{\partial^2 A}{\partial x^2} + SA^2 - (\mu + \rho)A, \\ \frac{\partial S}{\partial t} &= D_S \frac{\partial^2 S}{\partial x^2} - SA^2 + \rho(1 - S). \end{split} \tag{32}$$

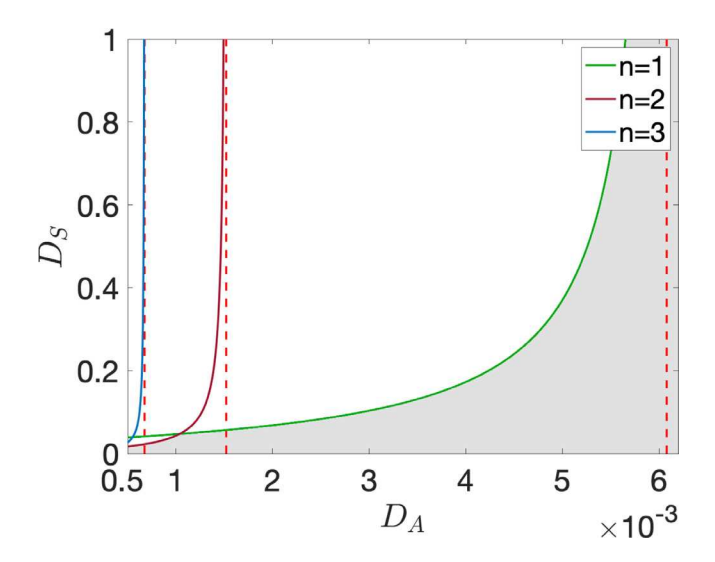


**Fig. 4.** The relationship between  $(D_S)_n^1$  and  $D_A$  from Eq. (41) with  $A_1^* = 3/5$ . Dashed curves indicate asymptotes. Curves with different colors represent different bifurcation branches. The number of bifurcation points is equal to the number of intersections with a vertical line. The constant solution  $(A_1^*, S_1^*) = (\frac{3}{5}, \frac{1}{10})$  is linearly stable within the shaded region. Other parameter values used are:  $\mu = 0.02$  and  $\rho = 0.04$ .

Here A and S represent the concentration of an activator and a substrate, respectively. The parameters  $D_A$  and  $D_S$  are the diffusion rates. The dynamics of the system correspond to the following reactions,

$$S + 2A \xrightarrow{1} 3A$$
,  $A \xrightarrow{\mu} P$ 

where P is a terminal product. In addition, the substrate S is fed into the system with a constant rate  $\rho$ , and both S and A undergo a linear decay at the same rate  $\rho$ .

The bifurcation and stability analysis of the Gray-Scott model have been extensively explored in [43–46]. In this section, we will apply the same framework to analyze Gray-Scott model. In order to make the system (32) resemble (1) with  $D_u=1$  and  $D_v=d$ , we make a change of variables. Denote

$$\bar{t} = D_A t, \qquad \bar{A}(x, \bar{t}) = A(x, t), \qquad \bar{S}(x, \bar{t}) = S(x, t).$$

By omitting the bars in the notation, we can rewrite the new system as:

$$\begin{split} \frac{\partial A}{\partial t} &= \frac{\partial^2 A}{\partial x^2} + \frac{1}{D_A} \Big( SA^2 - (\mu + \rho)A \Big), \\ \frac{\partial S}{\partial t} &= d \frac{\partial^2 S}{\partial x^2} + \frac{1}{D_A} \Big( -SA^2 + \rho(1 - S) \Big), \end{split} \tag{33}$$

where the parameter  $d=\frac{D_S}{D_A}$  measures the ratio of two diffusion coefficients. Using the framework of (1), we have

$$f(A,S) = \frac{1}{D_A} \left( SA^2 - (\mu + \rho)A \right),$$
  
$$g(A,S) = \frac{1}{D_A} \left( -SA^2 + \rho(1-S) \right),$$

and hence

$$f_A(A,S) = \frac{1}{D_A} \Big( 2AS - (\mu + \rho) \Big),$$
 (34)

$$f_S(A,S) = \frac{1}{D_A} A^2,$$
 (35)

$$g_A(A,S) = \frac{-2}{D_A} AS, \tag{36}$$

$$g_S(A, S) = \frac{1}{D_A} \left( -A^2 - \rho \right).$$
 (37)

It is straightforward to see that  $(A^*, S^*) = (0, 1)$  is a constant steady-state solution for the system (33). Evaluating (34)–(37) at this constant

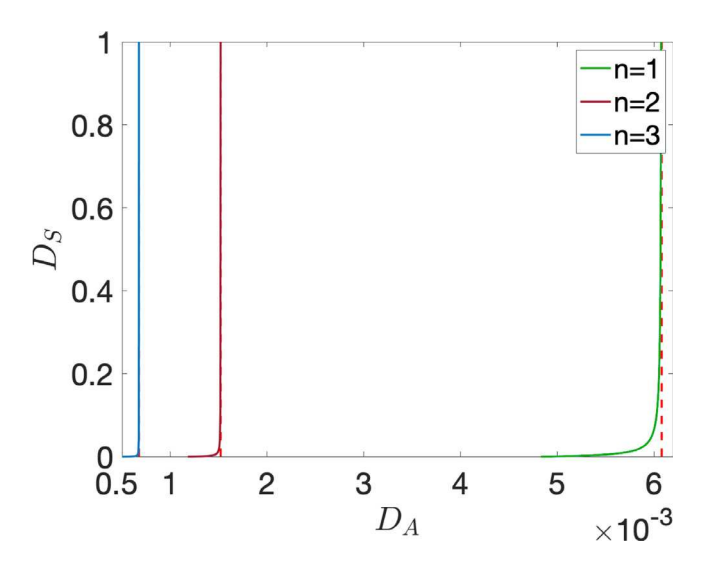


**Fig. 5.** The relationship between  $(D_S)_n^2$  and  $D_A$  from Eq. (41) with  $A_2^* = 1/15$ . Dashed curves indicate asymptotes. Curves with different colors represent different bifurcation branches. The number of bifurcation points is equal to the number of intersections with a vertical line. The constant solution  $(A_2^*, S_2^*) = (\frac{1}{15}, \frac{9}{10})$  is always unstable. Other parameter values used are:  $\mu = 0.02$  and  $\rho = 0.04$ .

solution, we obtain

$$f_A(0,1) = -\frac{\mu + \rho}{D_A}, \qquad f_S(0,1) = g_A(0,1) = 0, \qquad g_S(0,1) = -\frac{\rho}{D_A}.$$

By applying Theorem 2.1, we can determine the values of the bifurcation points as  $d_n^* = -\frac{\rho}{D_A n^2 \pi^2}$ . Since these values are negative. Therefore, we conclude that there are no non-constant steady-state solutions bifurcating from the trivial solution  $(A^*, S^*) = (0, 1)$ . In fact, by further employing Theorem 2.2, we can confirm that the constant solution  $(A^*, S^*) = (0, 1)$  is always stable.

In addition to the trivial solution  $(A^*, S^*) = (0, 1)$ , if  $\rho^2 - 4\rho(\mu + \rho)^2 > 0$ , there are two more constant steady states

$$(A_{1,2}^*,S_{1,2}^*) = \left(\frac{\rho \pm \sqrt{\rho^2 - 4\rho(\mu + \rho)^2}}{2(\mu + \rho)}, \frac{\rho \mp \sqrt{\rho^2 - 4\rho(\mu + \rho)^2}}{2\rho}\right), \tag{38}$$

and in this case, we have

$$A_{1,2}^* S_{1,2}^* = \mu + \rho. \tag{39}$$

At these two steady-state solutions, we apply Theorem 2.1 in conjunction with Eqs. (34)–(37). By also utilizing the property defined by (39), we can simplify our calculations and derive the formula for the bifurcation points

$$d_{n}^{*} = \frac{\frac{2(A_{1,2}^{*})^{3}S_{1,2}^{*}}{2A_{1,2}^{*}S_{1,2}^{*} - (\mu+\rho) - D_{A}n^{2}\pi^{2}} - (A_{1,2}^{*})^{2} - \rho}{D_{A}n^{2}\pi^{2}} = \frac{\frac{2(\mu+\rho)(A_{1,2}^{*})^{2}}{(\mu+\rho) - D_{A}n^{2}\pi^{2}} - (A_{1,2}^{*})^{2} - \rho}{D_{A}n^{2}\pi^{2}}.$$

$$(40)$$

Recall that  $d = \frac{D_S}{D_A}$  is the ratio of the two diffusion rates. If we view  $D_S$  as the bifurcation parameter, then bifurcation branches occur at

$$D_S = (D_S)_n^{1,2} = \frac{\frac{2(\mu+\rho)(A_{1,2}^*)^2}{(\mu+\rho)-D_A n^2 \pi^2} - (A_{1,2}^*)^2 - \rho}{n^2 \pi^2} \qquad n \ge 1.$$
 (41)

Similar to the analysis in Chapter 3, we shall discuss the number of bifurcation points based on the values of  $\mu, \rho$ , and  $D_A$ . In (41),  $(D_A)_n^* = \frac{\mu + \rho}{n^2 \pi^2}$  are the asymptotes, separating positive and negative values. In addition, for fixed n,  $(D_S)_n^{1,2}$  is monotonically increasing in  $D_A$ . Therefore, we obtain

• If the values of the bifurcation points defined in (41) stay positive in  $D_A \in (\frac{\mu+\rho}{(n+1)^2\pi^2}, \frac{\mu+\rho}{n^2\pi^2})$ , then there are n bifurcation points when

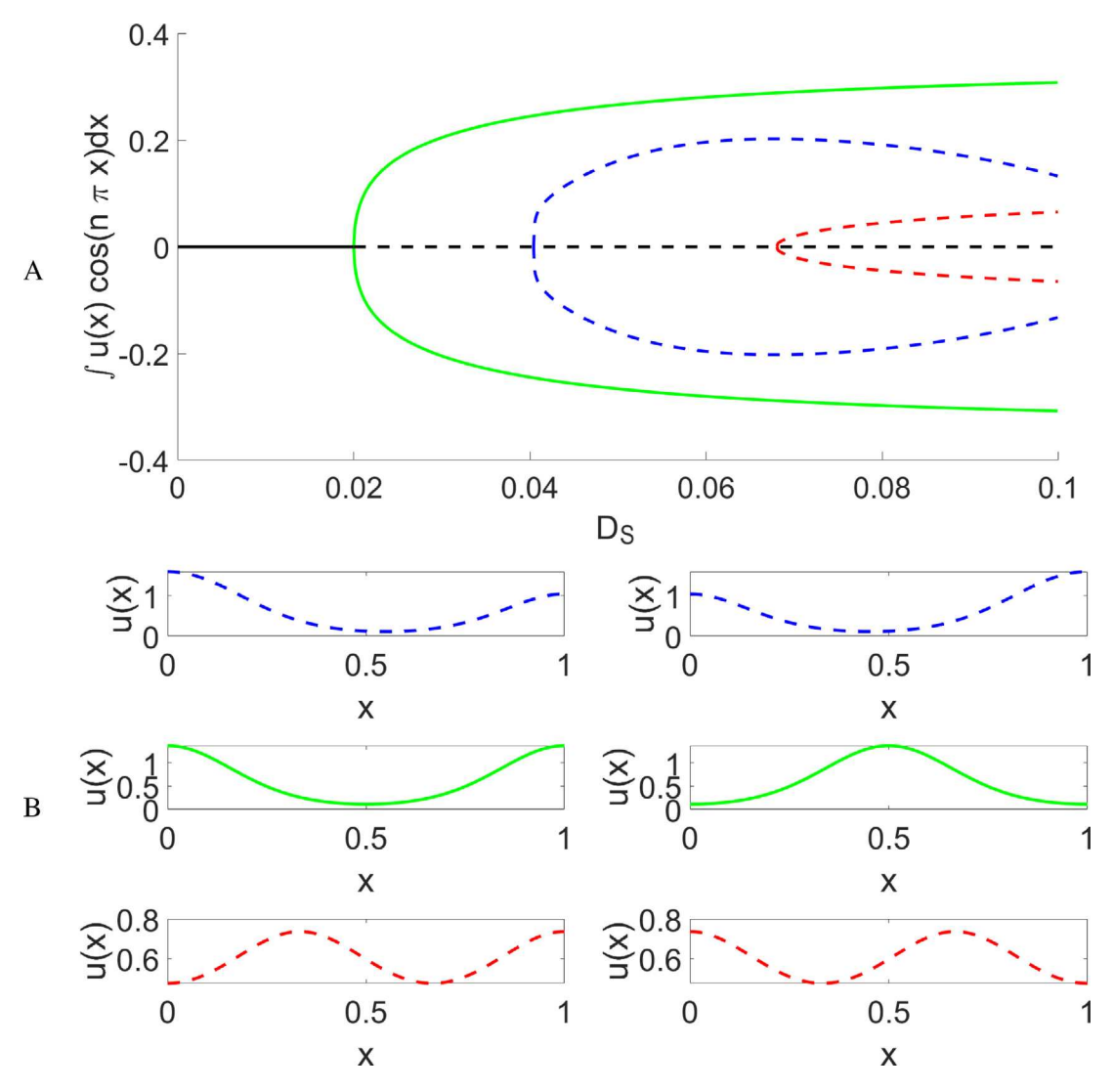


**Fig. 6.** Steady states of the Gray-Scott model around the constant solution  $(A_1^*, S_1^*) = (\frac{3}{5}, \frac{1}{10})$  with  $D_A = 6 \times 10^{-4}$ ,  $\mu = 0.02$ , and  $\rho = 0.04$ . A: Bifurcation diagram of the model. The *y*-axis represents  $\int u(x) \cos(n\pi x) \, dx$ , where u(x) are steady-state solutions. Solid lines indicate stable solutions, while dashed lines indicate unstable solutions. B: Steady-state solutions with  $D_S = 0.1$  for each solution branch distinguished by different colors.

 $\frac{\mu+\rho}{(n+1)^2\pi^2} \leq D_A < \frac{\mu+\rho}{n^2\pi^2}.$  There are no bifurcation points when  $D_A \geq \frac{\mu+\rho}{n^2}.$  An example of this case is shown in Fig. 4.

• If the values of the bifurcation points defined in (41) change signs in  $D_A \in (\frac{\mu+\rho}{(n+1)^2\pi^2},\frac{\mu+\rho}{n^2\pi^2})$ , then there is only one bifurcation point as long as the value computed by (41) is positive. There are no bifurcation points when  $D_A \geq \frac{\mu+\rho}{\pi^2}$ . An example of this case is shown in Fig. 5.

Since the value of  $(D_A)_n^* = \frac{\mu + \rho}{n^2 \pi^2} \to 0$  as  $n \to \infty$ , the number of asymptotes increases as  $D_A \to 0$ . Correspondingly, in the first case, the number of bifurcation points also increases as  $D_A \to 0$ .

When  $\mu=0.02$  and  $\rho=0.04$ , we obtain from (38) the other two constant steady states

$$(A_1^*, S_1^*) = \left(\frac{3}{5}, \frac{1}{10}\right) \text{ and } (A_2^*, S_2^*) = \left(\frac{1}{15}, \frac{9}{10}\right).$$

Figs. 4 and 5 show the relationship between the bifurcation point  $(D_S)_n^{1,2}$  and the activator's diffusion coefficient  $D_A$  at these two constant solutions, respectively. In these two figures, the number of bifurcation points at each  $D_A$  value is equal to the number of intersections with the vertical line  $x=D_A$ .

We combine Theorem 2.2 with (34)–(37), and also recall (39), to explore the stability of these two constant solutions. The two conditions from Theorem 2.2 are equivalent to, for all integers  $n \ge 0$ ,

$$\begin{split} \lambda_1 + \lambda_2 &= -n^2 \pi^2 + f_A(A^*, S^*) - \frac{D_S}{D_A} n^2 \pi^2 + g_S(A^*, S^*) \\ &= -n^2 \pi^2 + \frac{1}{D_A} \left( 2A^* S^* - (\mu + \rho) \right) - \frac{D_S}{D_A} n^2 \pi^2 + \frac{1}{D_A} \left( -(A^*)^2 - \rho \right) \\ &= -n^2 \pi^2 - \frac{D_S}{D_A} n^2 \pi^2 + \frac{1}{D_A} \left( \mu - (A^*)^2 \right) < 0, \end{split}$$

$$\tag{42}$$

$$\begin{split} \lambda_1 \lambda_2 &= \left[ -n^2 \pi^2 + \frac{1}{D_A} \left( 2A^* S^* - (\mu + \rho) \right) \right] \left[ -\frac{D_S}{D_A} n^2 \pi^2 - \frac{1}{D_A} \left( (A^*)^2 + \rho \right) \right] \\ &+ \frac{2}{(D_A)^2} (A^*)^3 S^* \\ &= \frac{1}{(D_A)^2} \left[ \left( -D_A n^2 \pi^2 + (\mu + \rho) \right) \left( -D_S n^2 \pi^2 - (A^*)^2 - \rho \right) \\ &+ 2(\mu + \rho) (A^*)^2 \right] > 0. \end{split}$$

(43)

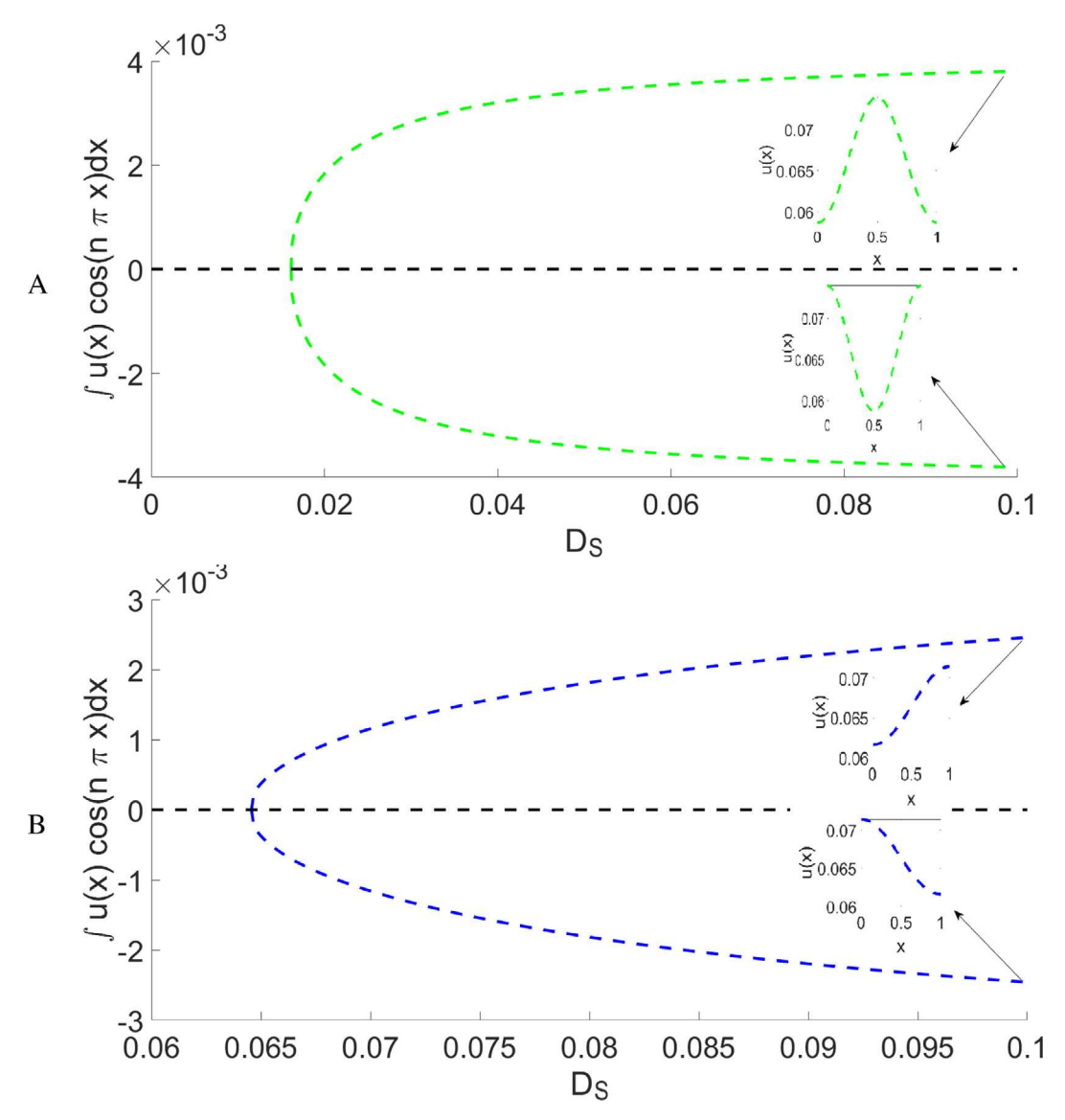


Fig. 7. Steady states of the Gray-Scott model with around constant solution  $(A_2^*, S_2^*) = (\frac{1}{15}, \frac{9}{10})$  with  $\mu = 0.02$  and  $\rho = 0.04$ . Dashed lines indicate unstable solutions. A: Bifurcation diagram and the nonuniform steady-state solution on the n = 2 bifurcation branch when  $D_A = 1.5 \times 10^{-3}$ . B: Bifurcation diagram and the nonuniform steady-state solution on the n = 1 bifurcation branch when  $D_A = 6 \times 10^{-3}$ .

Evaluating these two conditions at the steady states  $(A_1^*, S_1^*)$  and  $(A_1^*, S_2^*)$ , we obtain

• At  $(A_1^*, S_1^*) = (\frac{3}{5}, \frac{1}{10})$ , we notice that  $\mu - (A_1^*)^2 = 0.02 - (3/5)^2 < 0$  and  $(\mu + \rho)(-(A_1^*)^2 - \rho) + 2(\mu + \rho)(A_1^*)^2 = (\mu + \rho)((A_1^*)^2 - \rho) > 0$ . Hence, the condition (42) is always true for all  $n \ge 0$ , and (43) holds when n = 0. In addition, the bifurcation points  $(D_S)_n^1$  defined in (41) are the points that make the left-hand side of (43) equal to 0 for each integer  $n \ge 1$ . Similar to the analysis of the Schnakenberg model, we define

$$D_S^*(D_A) = \min_{n \ge 1} (D_S)_n^1, \tag{44}$$

i.e.,  $D_S^*$  is the smallest bifurcation point. It can be easily proved that  $D_S^*(D_A)$  is the critical value at which the constant solution  $(A_1^*, S_1^*)$  changes stability. To be more specific, when  $D_S < D_S^*(D_A)$ , the solution  $(A_1^*, S_1^*)$  is linearly stable (see the shaded region in Fig. 4); whereas when  $D_S > D_S^*(D_A)$ , the solution is unstable.

• At  $(A_2^*, S_2^*) = (\frac{1}{15}, \frac{9}{10})$ , we have  $\mu - (A_2^*)^2 = 0.02 - (1/15)^2 > 0$ . The first condition (42) is violated when n = 0 since

$$\lambda_1 + \lambda_2 \Big|_{n=0} = \frac{1}{D_A} \left( \mu - (A_2^*)^2 \right) > 0.$$
 (45)

Based on Theorem 2.2, the constant solution  $(A_2^*, S_2^*)$  is always unstable.

We then proceed to conduct numerical simulations to investigate the steady-state solutions of the Gray-Scott model in a 1D domain, with x ranging from 0 to 1 and subject to no-flux boundary conditions. Initially, we set the parameter values to  $D_A=6\times 10^{-4},~\mu=0.02,$  and  $\rho=0.04,$  while considering the trivial steady-state values of  $(A_1^*,S_1^*)=(\frac{3}{5},\frac{1}{10}).$  As illustrated in Fig. 6A, three distinct bifurcation points corresponding to n=1,~n=2, and n=3 are evident. This observation aligns with the findings in Fig. 4, which also identifies three bifurcation points for  $D_A=6\times 10^{-4}.$  Furthermore, solid lines represent stable solutions, while dashed inso depict unstable ones. Notably, the steady-state solution  $(A,S)=(\frac{3}{5},\frac{1}{10})$  remains stable before reaching the

first bifurcation point, consistent with Fig. 4. In Fig. 6B, we present the steady-state solutions with  $D_S=0.1$  for various bifurcation modes.

We further examine the bifurcation solutions near the trivial solution  $(A_2^*, S_2^*) = (\frac{1}{15}, \frac{9}{10})$  with the same values of  $\mu$  and  $\rho$ . Initially, we set  $D_A = 1.5 \times 10^{-3}$ . As observed in Fig. 5,  $D_A = 1.5 \times 10^{-3}$  corresponds to a unique intersection with the n=2 curve, which indicates a single bifurcation point. The bifurcation diagram from the numerical simulation is shown in Fig. 7A and the nonuniform steady-state solutions are plotted when  $D_S = 0.1$ . It is evident that there is only one bifurcation point and steady-state solutions in this case resemble the graph of  $\cos(2\pi x)$  in the interval [0,1]. Subsequently, we consider the scenario with  $D_A = 6 \times 10^{-3}$ . This time, the unique intersection observed in Fig. 5 is between the vertical line  $D_A = 6 \times 10^{-3}$  and the curve for n=1. The simulation outcomes shown in Fig. 7B reveal that the nonuniform steady-state solutions in this case are on the n=1 bifurcation branch.

#### 5. Discussion

The central challenge in developmental biology is to decipher the mechanisms that govern the emergence of spatial and temporal patterns in living organisms. Mathematical modeling is an indispensable tool in this endeavor. However, the complexity of biological systems often results in the existence of nonuniform steady states, which pose challenges for mathematical characterization. In this paper, we investigated whether nontrivial steady states can bifurcate from trivial ones, contributing to the understanding of these systems' solution structures. Our methodology involved applying bifurcation and stability analyses to a general reaction—diffusion system featuring two species, from which we derived nontrivial solution branches that bifurcate from the trivial ones. Utilizing the Crandall—Rabinowitz theorem, we identified bifurcation points where nonuniform steady-state solutions emerge from the trivial solution.

The methods developed in this paper can be readily applied to analyze reaction–diffusion models with n species. Similar results as Theorems 2.1 and 2.2 can be obtained except that the analysis will be based on an  $n \times n$  matrix, and the computation of deriving the determinant and eigenvalues of the  $n \times n$  matrix will be more involved.

We applied our methods to two classic models in mathematical biology: the Schnakenberg Turing model, and the Gray–Scott model. For both models, our theoretical results are consistent with numerical simulations. The implications of our findings extend beyond these specific models. Understanding how nontrivial states emerge from trivial ones is a fundamental question in biology and mathematics. Our approach not only contributes to our knowledge of biological pattern formation but also opens the door to further applications in more complex systems.

## CRediT authorship contribution statement

**Xinyue Evelyn Zhao:** Formal analysis, Methodology, Writing – original draft, Writing – review & editing. **Wenrui Hao:** Conceptualization, Methodology, Software, Writing – original draft, Writing – review & editing.

# Declaration of competing interest

The authors declare the following financial interests/personal relationships which may be considered as potential competing interests: Wenrui Hao reports financial support was provided by National Institutes of Health. Wenrui Hao reports financial support was provided by National Science Foundation.

# Acknowledgments

WH is supported by NIH, United States via 1R35GM146894 and NSF DMS-2052685. The authors are grateful to the reviewers for their careful review and helpful suggestions.

#### References

- A. Gierer, H. Meinhardt, A theory of biological pattern formation, Kybernetik 12 (1972) 30–39.
- [2] L. Hall-Stoodley, P. Stoodley, Developmental regulation of microbial biofilms, Curr. Opin. Biotechnol. 13 (3) (2002) 228–233.
- [3] J.D. Murray, Mathematical biology: I. An introduction. Interdisciplinary applied mathematics, in: Mathematical Biology, vol. 17, Springer, 2002.
- [4] A.M. Turing, The chemical basis of morphogenesis, Bull. Math. Biol. 52 (1990) 153–197.
- [5] H.G. Othmer, K. Painter, D. Umulis, C. Xue, The intersection of theory and application in elucidating pattern formation in developmental biology, Math. Model. Nat. Phenom. 4 (4) (2009) 3–82.
- [6] J.E. Pearson, Complex patterns in a simple system, Science 261 (5118) (1993) 189–192.
- [7] J. Wang, J. Shi, J. Wei, Dynamics and pattern formation in a diffusive predatorprey system with strong Allee effect in prey, J. Differential Equations 251 (4–5) (2011) 1276–1304.
- [8] J.L. Aragón, R.A. Barrio, T.E. Woolley, R.E. Baker, P.K. Maini, Nonlinear effects on Turing patterns: Time oscillations and chaos, Phys. Rev. E 86 (2) (2012) 026201.
- [9] S. Kondo, T. Miura, Reaction-diffusion model as a framework for understanding biological pattern formation, Science 329 (5999) (2010) 1616–1620.
- [10] S. Zhao, J. Ovadia, X. Liu, Y.T. Zhang, Q. Nie, Operator splitting implicit integration factor methods for stiff reaction-diffusion-advection systems, J. Comput. Phys. 230 (15) (2011) 5996–6009.
- [11] C.T. Kelley, Iterative Methods for Linear and Nonlinear Equations, SIAM, 1995.
- [12] W.C. Lo, L. Chen, M. Wang, Q. Nie, A robust and efficient method for steady state patterns in reaction-diffusion systems, J. Comput. Phys. 231 (15) (2012) 5062–5077.
- [13] J. Xu, L. Zikatanov, Algebraic multigrid methods, Acta Numer. 26 (2017) 591–721.
- [14] P.E. Farrell, A. Birkisson, S.W. Funke, Deflation techniques for finding distinct solutions of nonlinear partial differential equations, SIAM J. Sci. Comput. 37 (4) (2015) A2026–A2045.
- [15] W. Hao, C. Xue, Spatial pattern formation in reaction-diffusion models: a computational approach, J. Math. Biol. 80 (2020) 1–23.
- [16] W. Hao, J.D. Hauenstein, B. Hu, A.J. Sommese, A bootstrapping approach for computing multiple solutions of differential equations, J. Comput. Appl. Math. 258 (2014) 181–190.
- [17] W. Hao, J. Hesthaven, G. Lin, B. Zheng, A homotopy method with adaptive basis selection for computing multiple solutions of differential equations, J. Sci. Comput. 82 (2020) 1–17.
- [18] L. Yang, M. Dolnik, A.M. Zhabotinsky, I.R. Epstein, Pattern formation arising from interactions between Turing and wave instabilities, J. Chem. Phys. 117 (15) (2002) 7259–7265.
- [19] M.G. Neubert, H. Caswell, J.D. Murray, Transient dynamics and pattern formation: reactivity is necessary for Turing instabilities, Math. Biosci. 175 (1) (2002)
- [20] D. Iron, J. Wei, M. Winter, Stability analysis of Turing patterns generated by the Schnakenberg model, J. Math. Biol. 49 (2004) 358–390.
- [21] M.G. Crandall, P.H. Rabinowitz, Bifurcation from simple eigenvalues, J. Funct. Anal. 8 (2) (1971) 321–340.
- [22] L. Nirenberg, Topics in Nonlinear Functional Analysis, vol. 6, American Mathematical Soc., 1974.
- [23] X.E. Zhao, L.Q. Chen, W. Hao, Y. Zhao, Bifurcation analysis reveals solution structures of phase field models, Commun. Appl. Math. Comput. (2022) 1–26.
- [24] G. Webb, X.E. Zhao, Bifurcation analysis of critical values for wound closure outcomes in wound healing experiments, J. Math. Biol. 86 (5) (2023) 66.
- [25] H. Fujii, M. Mimura, Y. Nishiura, A picture of the global bifurcation diagram in ecological interacting and diffusing systems, Physica D 5 (1) (1982) 1–42.
- [26] J. Jang, W.M. Ni, M. Tang, Global bifurcation and structure of Turing patterns in the 1-D Lengyel-Epstein model, J. Dynam. Differential Equations 16 (2004) 297–320.
- [27] Y. Nishiura, Global structure of bifurcating solutions of some reaction-diffusion systems, SIAM J. Math. Anal. 13 (4) (1982) 555–593.
- [28] J. Shi, Bifurcation in infinite dimensional spaces and applications in spatiotemporal biological and chemical models, Front. Math. China 4 (2009) 407–424.
- [29] J. Jin, J. Shi, J. Wei, F. Yi, Bifurcations of patterned solutions in the diffusive Lengyel-Epstein system of CIMA chemical reactions, Rocky Mountain J. Math. (2013) 1637–1674.
- [30] F. Yi, J. Wei, J. Shi, Bifurcation and spatiotemporal patterns in a homogeneous diffusive predator-prey system, J. Differential Equations 246 (5) (2009) 1944–1977.
- [31] M.G. Crandall, P.H. Rabinowitz, Bifurcation, perturbation of simple eigenvalues and linearized stability. Arch. Ration. Mech. Anal. 52 (1973) 161–180.
- [32] A. Friedman, B. Hu, Bifurcation from stability to instability for a free boundary problem arising in a tumor model, Arch. Ration. Mech. Anal. 180 (2006) 293–330.

- [33] A. Friedman, B. Hu, Stability and instability of Liapunov-Schmidt and Hopf bifurcation for a free boundary problem arising in a tumor model, Trans. Amer. Math. Soc. 360 (10) (2008) 5291–5342.
- [34] Y. Huang, Z. Zhang, B. Hu, Bifurcation from stability to instability for a free boundary tumor model with angiogenesis., Discrete Contin. Dyn. Syst. Ser. A 39 (5) (2019).
- [35] W. Hao, An adaptive homotopy tracking algorithm for solving nonlinear parametric systems with applications in nonlinear ODEs, Appl. Math. Lett. (2021) 107767.
- [36] W. Hao, C. Zheng, An adaptive homotopy method for computing bifurcations of nonlinear parametric systems, J. Sci. Comput. 82 (3) (2020) 1–19.
- [37] W. Hao, C. Zheng, A stochastic homotopy tracking algorithm for parametric systems of nonlinear equations, J. Sci. Comput. 87 (3) (2021) 1–14.
- [38] M. Gentile, A. Tataranni, Turing instability for the Schnackenberg system, in: Proceedings "Waves and Stability in Continuous Media", 2008, pp. 309–314.
- [39] P. Liu, J. Shi, Y. Wang, X. Feng, Bifurcation analysis of reaction-diffusion Schnakenberg model, J. Math. Chem. 51 (8) (2013) 2001–2019.

- [40] P. Gray, S.K. Scott, Autocatalytic reactions in the isothermal, continuous stirred tank reactor: isolas and other forms of multistability, Chem. Eng. Sci. 38 (1) (1983) 29–43.
- [41] P. Gray, S.K. Scott, Autocatalytic reactions in the isothermal, continuous stirred tank reactor: Oscillations and instabilities in the system A+ 2B→ 3B; B→ C, Chem. Eng. Sci. 39 (6) (1984) 1087–1097.
- [42] P. Gray, S.K. Scott, Sustained oscillations and other exotic patterns of behavior in isothermal reactions, J. Phys. Chem. 89 (1) (1985) 22–32.
- [43] A. Doelman, T.J. Kaper, P.A. Zegeling, Pattern formation in the one-dimensional Gray-Scott model, Nonlinearity 10 (2) (1997) 523.
- [44] X. Wang, J. Shi, G. Zhang, Bifurcation and pattern formation in diffusive Klausmeier-Gray-Scott model of water-plant interaction, J. Math. Anal. Appl. 497 (1) (2021) 124860.
- [45] J. Wei, Existence, stability and metastability of point condensation patterns generated by the Gray-Scott system, Nonlinearity 12 (3) (1999) 593.
- [46] J. Wei, Pattern formations in two-dimensional Gray-Scott model: existence of single-spot solutions and their stability, Physica D 148 (1-2) (2001) 20-48.